Bulletin of the Seismological Society of America, 90, 3, pp. 655–665, June 2000

The Energy Partitioning and the Diffusive Character of the Seismic Coda

by N. M. Shapiro, M. Campillo, L. Margerin, S. K. Singh, V. Kostoglodov, and J. Pacheco

Abstract Following recent theoretical developments of the radiative transfer theory of elastic waves, we propose to use the ratio R of energies of curl and divergence part of the ground displacement to distinguish between the different possible dominant scattering regimes in the lithosphere. A consequence of the diffusion regime is the partitioning of the energy between different vibrational modes, which is independent of time. It results in the stabilization of R. This behavior is not expected if low-order diffraction (such as single scattering) is dominant. We apply our technique to seismograms recorded by a small-aperture seismic array operated during June–August 1997 in Guerrero (Mexico). We estimate the energy ratio R in the coda of 13 earthquakes recorded by the array. We find it to be very stable in the coda window, while the energy level itself changes by several orders of magnitude. The value of R is 7 ± 1, independent of the earthquake location and the magnitude. The observed stabilization of R is a strong indication of the diffusive regime of the seismic coda.

Introduction

Since the pioneering study by Aki (1969), it is widely recognized that the coda of seismic signals is composed of waves scattered by small-scale heterogeneities in the Earth. The most prominent property of the seismic coda is that its envelope decreases at long lapse times with a rate that is independent of the seismic source and is constant for a given site. This observation has been made in different regions of the Earth. See Campillo *et al.* (1999) and Sato and Fehler (1998) for references. This stability of the exponential form required to express the decay led to the estimation of the "coda quality factor," Q_c. The value of Q_c has been measured for many regions of the Earth. These measurements have been used to infer the inelastic attenuation in the Earth's crust and the statistical description of the distribution of small-scale heterogeneities. The interpretation of Q_c measurements is based on the theory of the scattering of seismic waves. However, different approximations used to describe the coda give rise to different interpretations of Q_c. The scalar single scattering approximation (Aki and Chouet, 1975) supposes that the seismic coda is composed of first-order scattered S waves. In this case, the coda quality factor is equal to the quality factor of direct S waves, which is given by:

$$1/Q_c = 1/Q_i + 1/Q_s \tag{1}$$

where Q_i and Q_s are intrinsic and scattering quality factors, respectively. This approximation has been used in numerous studies to infer the attenuation of S waves. Aki and Chouet have also considered the possibility of multiple scattering through its asymptotic form, that is, the diffusion approximation in a homogeneous space. In this case, Q_c represents mostly the inelastic attenuation:

$$Q_c = Q_i \tag{2}$$

Wu (1985) introduced the stationary radiative transfer equation for scalar waves. Abubakirov and Gusev (1990) and Hoshiba (1991) used the Monte Carlo method to solve this equation in the time domain. In these studies, a constant background velocity and a homogeneous distribution of scatterers were assumed. The use of this type of model in the interpretation of the observed Q_c suggests that the coda decay is dominated by the intrinsic absorption and that this absorption exhibits a strong frequency dependence. During the last few years, models with a more realistic distribution of scatterers and seismic-wave velocities have been considered (Gusev, 1995; Hoshiba, 1997; Margerin *et al.,* 1998). Margerin *et al.* (1999) and Campillo *et al.* (1998) studied the effect of the Moho discontinuity on the form of the coda envelopes by solving the radiative transfer equations in a model containing a heterogeneous layer overlying a transparent half-space. They found that, at high frequencies ($f \geq 10$ Hz), Q_c is dominated by the intrinsic absorption, while at frequencies around 1 Hz, it can be dominated by the effect of the leakage of the diffuse seismic energy in the mantle. Thus at frequencies $\sim$1 Hz, Q_c depends strongly on the mean free path of the seismic waves in the crust and on the crustal thickness. Q_c at low frequency is therefore expected to have strong regional variations, correlated with both the degree of heterogeneity of the crust and the crustal thickness, as it is observed.

As we can see, the interpretation of the coda Q measurements in terms of the properties of the Earth material leads to dramatically different results when using different theories of wave scattering or assumption of different scattering regimes. Most of the previous theoretical studies of the seismic coda have used the acoustic approximation and did not consider different wave polarizations and mode conversions. As a consequence, the experimental studies were essentially concerned with the measurement of the decay rate of the coda envelopes. However, such measurements are insufficient to distinguish unambiguously different scattering regimes, since all approximations predict the exponential coda decay. Recently, the elastic radiative transfer equation has been derived (Weaver, 1990; Papanicolaou *et al.,* 1996; Ryzhik *et al.,* 1996). This equation takes into account the wave polarization and the mode conversion between P and S waves, which occurs during each scattering event. One of the fundamental results is that, in the diffusion regime, the ratio R of energy densities of S to P waves becomes a constant:

$$\frac{W_s}{W_p} = \frac{2\alpha^3}{\beta^3} \tag{3}$$

where α and β denote the P- and S-wave velocity, respectively. This property can be regarded simply as a complete randomization of the wave field in the phase domain. In other words, the total energy follows a single diffusion equation and, consequently, P- and S-wave energies have the same time evolution. For a medium with $\alpha/\beta = \sqrt{3}$, the ratio (3) equals 10.4. This value can be slightly changed if an anelastic attenuation is present in the media. However, the energy densities of the P and the S waves remain equipartitioned in this case (Margerin *et al.,* 2000b).

Margerin *et al.* (2000a) solved the elastic radiative transfer equation using a Monte Carlo method. They have also obtained the energy partitioning in the diffusive regime. Moreover, it has been shown that the time required to reach the diffusive regime and equipartitioning strongly depends on the mechanism of scattering, that is, on the ratio of a characteristic dimension of the heterogeneity to the wavelength. Thus, the measurement of the energy partition in the seismic coda can give a very strong indication on the regime of seismic-wave scattering in the Earth. The difficulty arises in measuring the partitioning of the energy, since in the coda, different types of waves cannot be separated from ground-motion records at a single point. Applying a frequency-wave number analysis to the data of the NORSAR array, Dainty and Toksoz (1990) have shown that the coda is dominated by waves with apparent velocities less than 4 km/sec, that is, by S waves. However, they could not quantify the energy density ratio. In this article, we present another approach based on the processing of the data from a small-aperture array. It relies on the measurement of spatial derivatives and calculation of curl and divergence of the displacement. We can estimate energy of P and S waves separately using the fact that

$$\operatorname{curl} \vec{u} = 0 \tag{4}$$

for P wave and

$$\operatorname{div} \vec{u} = 0 \tag{5}$$

for S waves.

We installed and operated a small-aperture array in the region of Chilpancingo, Guerrero, Mexico, during June–August 1997. The array consisted of four stations installed at the corners of a square with a side of $\sim$ 50 m. During the period of the experiment, we recorded 13 events with high signal-to-noise ratio in the coda. In this article we present the analysis of the data and the implications of our observations on the scattering regime of seismic-coda waves.

Diffusive Wave Field and Energy Partitioning in an Infinite Space

The diffusion approximation appears as an asymptotic solution of the radiative transfer equation at large lapse times (Weaver, 1990; Ryzhik *et al.,* 1996). The main condition of validity of the radiative transfer equation is that the scattering mean free paths are much larger than the wavelengths, making it possible to neglect interference effects (Papanicolaou *et al.,* 1996). The diffusive regime is reached when the distribution of specific intensity is almost isotropic, which typically occurs after a few transport mean-free times. In other words, the achievement of the diffusive regime means the complete randomization of the wave field in the phase domain as a result of multiple scattering. Following Weaver (1982), we can use two simple definition of the diffusive wave field.

The first definition considers a diffuse field at a given frequency to be a state of excitation for which different normal modes of the system are in a statistical equilibrium, that is, the energy is equally distributed between all normal modes. Equation (3) can very easily be derived using this definition. It just requires the calculation of the number of P- and S-type normal modes per unit volume (Weaver, 1982).

The more usual definition demands that, at each point of the vibrating medium, the diffuse field can be represented as an isotropic and random superposition of plane waves. Each plane wave has a slowly time varying amplitude and a random phase. As a consequence, different plane waves and different displacement components are noncorrelated. We will use the plane-wave decomposition of the wave field to derive expressions for the energy densities of P and S waves. First, we can use the property of a plane wave that its kinetic and strain-energy densities are equal when both are averaged over one or more periods. Therefore, for our purposes it is sufficient to consider the strain energy. The

energy density, *W,* associated with the deformation in the solid medium is given by

$$W = \frac{1}{2}\,\sigma_{ij}\chi_{ij} \tag{6}$$

where χ is the strain tensor and σ is the stress tensor. In Appendix A, we show that, in an isotropic medium, equation (6) can be rewritten as:

$$W = \left(\frac{\lambda}{2} + \mu\right)(\mathrm{div}\,\vec{u})^2 + \frac{\mu}{2}(\mathrm{curl}\,\vec{u})^2 + \mu I \tag{7}$$

where u is the displacement, and λ and μ are Lame constants,

$$\begin{aligned} I = {} & 2\left(\frac{\partial u_x}{\partial y}\frac{\partial u_y}{\partial x} + \frac{\partial u_x}{\partial z}\frac{\partial u_z}{\partial x} + \frac{\partial u_y}{\partial z}\frac{\partial u_z}{\partial y}\right) \\ & - 2\left(\frac{\partial u_x}{\partial x}\frac{\partial u_y}{\partial y} + \frac{\partial u_x}{\partial x}\frac{\partial u_z}{\partial z} + \frac{\partial u_y}{\partial y}\frac{\partial u_z}{\partial z}\right). \end{aligned} \tag{8}$$

If we calculate the energy in a relatively large time window, the term I vanishes since it is composed of products of noncorrelated functions. Therefore, the average energy can be written as:

$$\bar{W} = \overline{W_P} + \overline{W_S} \tag{9}$$

where,

$$\overline{W_P} = \overline{\left(\frac{\lambda}{2} + \mu\right)(\mathrm{div}\,\vec{u})^2} \tag{10}$$

and

$$\overline{W_S} = \overline{\frac{\mu}{2}(\mathrm{curl}\,\vec{u})^2}. \tag{11}$$

Equations (10) and (11) can be used to estimate *P*- and *S*-wave energies separately using seismic sensors installed in closely spaced boreholes at different depths, relatively far from the Earth's surface. It would enable us to calculate the partial derivatives with respect to all three spatial coordinates required for the estimation of the *P*- and *S*-wave energies. However, the installation of numerous seismic stations in boreholes is extremely expensive. For this reason, we considered the possibility of computation of the energy partitioning using only sensors installed at the surface.

Energy Partitioning at the Earth's Surface

General Considerations

The separation of *P*- and *S*-wave energies proposed in the previous section can be performed only if the wave field can be represented as a sum of noncorrelated plane body waves. However, when our observation point is located close to the free surface, the simple model presented earlier is not adequate. The total wave field in this case is composed of the incident and the reflected body waves as well as the surface waves. The diffuse field close to the free surface of a medium with constant wave velocities has been studied by Weaver (1985). Using the normal mode definition of a diffuse wave field, he has shown that, at the surface, the energy is redistributed among *P, S*, and Rayleigh waves. This implies that the ratio between the energy densities of each of the three types of waves remains constant in the diffusive regime. Moreover, Weaver (1985) could evaluate the ratio of *P*- to *S*-energy densities and showed that it is still given by equation (3).

However, equations (10) and (11) cannot allow us to estimate the Rayleigh waves contribution, since for this wave type, both divergence and curl are nonzero. Moreover, close to the free surface, we cannot neglect the correlation between incident and reflected waves. This correlation can result in large errors in the energy density estimation using equations (10) and (11).

Energy of a Single Incident Plane Wave at the Surface

Let us consider the simple case of a plane *SH*-wave incident at the free surface of a homogeneous half-space with angle θ:

$$\mu_0 \cos\,\omega\left(\frac{\sin\,\theta}{\beta}\,x - \frac{\cos\,\theta}{\beta}\,z - t\right). \tag{12}$$

The amplitude of this wave is normalized to a unit energy density according to equation (11):

$$u_0 = \frac{2\rho}{\omega} \tag{13}$$

where ω is the frequency, β the *S*-wave speed, and ρ the density. The reflected wave can be expressed as:

$$u_0 \cos\,\omega\left(\frac{\sin\,\theta}{\beta}\,x + \frac{\cos\,\theta}{\beta}\,z - t\right). \tag{14}$$

Let us now calculate the energy of the total wave field through equations (10) and (11) at the free surface, that is, at $z = 0$. The *P*-wave energy will be 0 because the divergence is 0. However, the *S*-wave energy will strongly depend on the incident angle θ. For example, if $\theta = 0$, the combination of the incident reflected waves will result in a standing wave

$$2u_0 \cos\left(\frac{\omega}{\beta}\,z\right)\cos\,\omega t, \tag{15}$$

and at the free surface, all partial derivatives with respect to spatial coordinates equal 0. As a consequence, the rotational

component of the field and the measured energy vanish. If $\theta = \pi/2$, the incident and the reflected waves are completely in phase, and the measured energy density equals 4. The situation is more complicated if we consider the incidence of a plane *P* wave. In this case, there are two reflected waves: *P* and *SV*. For the total field, i.e., the sum of the three waves, both the divergence and curl are, in general, different from zero. As a consequence, for an incident *P* wave, we will measure nonzero *S*-wave energy. The situation is similar for the incidence of a plane *SV* waves. In this case we can measure a nonzero *P*-wave energy. Therefore, the presence of the free surface affects strongly the measurement of *P*- and *S*-wave energies using equations (10) and (11).

In order to quantify the influence of the surface on our measurements, we calculated the measured *P*- and *S*-wave energies for all types of incident waves (*P*, *SV*, *SH*) and for all values of the incident angle ($0 < \theta < \pi/2$). For each incident plane wave, we calculated the reflected waves using the expressions given by Aki and Richards (1980, p. 141). We then computed the divergence and curl for the sum of the direct and reflected waves. We applied equations (10) and (11) to calculate the apparent *S* and *P* energy measured at the surface. We define five energy reflection coefficients as the ratios of the energy density measured at the surface to the energy density of the incident wave field:

$$E_{P\to P}(\theta) \quad E_{P\to SV}(\theta) \quad E_{SV\to P}(\theta) \quad E_{SV\to SV}(\theta) \quad E_{SH\to SH}(\theta) \qquad (16)$$

These five coefficients correspond to all the possible wave-type conversions. We emphasize that these are not classical energy-reflection coefficients. Coefficients in equation (16) take into account the interference between incident and reflected waves at the free surface, and they give the ratio of the energy of the *S*- or *P*-wave energies measured at the surface to the energy of the incident plane wave in the bulk. The angular dependence of the coefficients calculated for a poissonian medium is shown in Figure 1.

The results show that, close to the free surface, the estimation of the energy of a single wave can be subject to very large errors. For example, let us consider a *P*-wave incident at the surface with a relatively small angle ($\theta < 40°$). As it can be seen from Figure 1, the *S*-wave energy density calculated using equation (11) will be much larger than the *P*-wave energy density calculated with equation (10). Thus, an incident *P* wave could appear as an *S* wave. Moreover, the calculated *S*-to-*P* energy density for a single wave depends strongly on the incident angle θ.

Effect of the Free Surface on the Measurement of Energy Partition

The discussion in the last paragraph does not imply, however, the impossibility of observing the energy partitioning of a diffusive wave field. Let us consider a random and isotropic wave-field incident at the surface. In this case we can define integrated energy coefficients as follows:

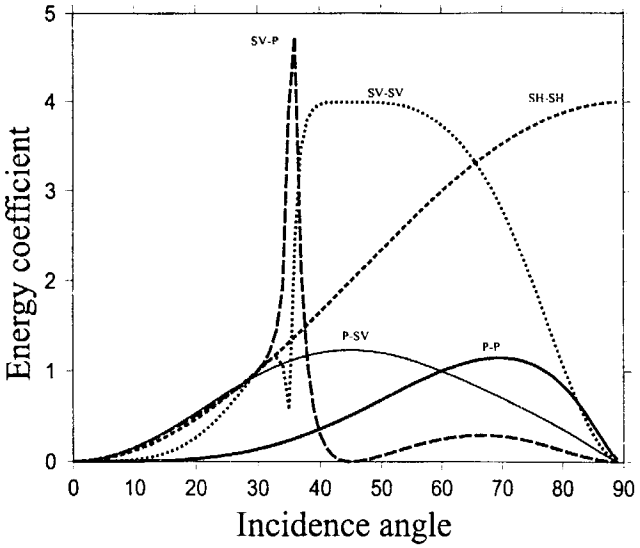

Figure 1. Apparent *P*- and *S*-wave energies measured at the surface for an incident plane wave.

$$W_{P\to P} = \int_0^{\frac{\pi}{2}} E_{P\to P}(\theta)\ \sin\ \theta d\theta$$

$$W_{P\to SV} = \int_0^{\frac{\pi}{2}} E_{P\to SV}(\theta)\ \sin\ \theta d\theta$$

$$W_{SV\to P} = \int_0^{\frac{\pi}{2}} E_{SV\to P}(\theta)\ \sin\ \theta d\theta \qquad (17)$$

$$W_{SV\to SV} = \int_0^{\frac{\pi}{2}} E_{SV\to SV}(\theta)\ \sin\ \theta d\theta$$

$$W_{SH\to SH} = \int_0^{\frac{\pi}{2}} E_{SH\to SH}(\theta)\ \sin\ \theta d\theta$$

These coefficients are simply the angular averages of the energy reflection coefficient defined previously. Coefficients (17) can be estimated numerically. For a poissonian medium we obtain $W_{P\to P} = 0.64$, $W_{P\to SV} = 0.75$, $W_{SV\to P} = 0.40$, $W_{SV\to SV} = 2.25$, $W_{SH\to SH} = 2.66$. Now assume that, in the incident field, the energy is equipartioned, that is, the *S*-to-*P* energy ratio ξ_0 is given by equation (3) and that the *SH* and *SV* energies are equal. The apparent *S*-to-*P* energy ratio ξ measured at the surface is simply obtained by weighting correctly the coefficients defined in (17).

$$\xi = \frac{\frac{\xi_0}{2} W_{SV\to SV} + \frac{\xi_0}{2} W_{SH\to SH} + W_{P\to SV}}{\frac{\xi_0}{2} W_{SV\to P} + W_{P\to P}} \qquad (18)$$

For a poissonian medium, equations (3) and (18) give $\xi \approx \xi_0 \approx 10$.

Two problems associated with the surface must still be

considered. The first is of an experimental nature. When we use receivers installed only at the Earth's surface, we cannot estimate directly the spatial derivatives with respect to the vertical coordinate. This difficulty can be overcome by using the free-surface boundary conditions. The condition of zero traction at the surface gives a system of equations that allows us to calculate the derivative along the vertical axis Z, as a function of the derivatives along two horizontal directions X and Y. A similar approach has already been used in the calculation of the strain associated with seismic waves using small-aperture arrays (Spudich *et al.,* 1995; Bodin *et al.,* 1997). Let us define R, the ratio of the curl to divergence energies at the surface. We show in Appendix B that R can be calculated using the following equation:

$$R = \frac{\overline{\frac{\mu}{2}(\mathrm{curl}\,\vec{u})^2}}{\overline{\left(\frac{\lambda}{2}+\mu\right)(\mathrm{div}\,\vec{u})^2}} = \frac{1}{4}\left(\frac{\alpha}{\beta}\right)^2 \frac{\overline{4\frac{\partial u_z{}^2}{\partial x} + 4\frac{\partial u_z{}^2}{\partial y} + \left(\frac{\partial u_x}{\partial y} - \frac{\partial u_y}{\partial x}\right)^2}}{\overline{\left(\frac{\partial u_x}{\partial x} + \frac{\partial u_y}{\partial y}\right)^2}}, \quad (19)$$

which includes only derivatives with respect to horizontal coordinates and therefore can be used to estimate the ratio R from an array of seismometers installed on the Earth's surface. In the following, the ratio R will be used to compute the energy partitioning in the seismic coda. It can be seen from equation (18) that, if our field consists only of body waves, we can expect $R \approx 10$. However, the presence of Rayleigh waves can change this value, and this is the second problem that needs to be discussed. Let us consider a plane Rayleigh wave propagating in the direction X:

$$u_z = \varepsilon \cos(\omega t - kx) \quad (20)$$

$$u_x = -\sin(\omega t - kx) \quad (21)$$

where w is the frequency, k is the horizontal wavenumber, and ε is the vertical-to-horizontal axis ratio. In this only the partial derivatives along x: $\frac{\partial u_z}{\partial x}$ and $\frac{\partial u_x}{\partial x}$ are nonzero and equation (19) becomes

$$R = \left(\frac{\alpha}{\beta}\right)^2 \frac{\overline{\frac{\partial u_z{}^2}{\partial x}}}{\overline{\frac{\partial u_x{}^2}{\partial x}}} = \left(\frac{\alpha}{\beta}\right)^2 \varepsilon^2 \quad (22)$$

For a poissonian medium, $(\alpha/\beta)^2 = 3$ and $\varepsilon = 1.47$. From equation (22), we obtain $R \approx 6.5$.

For a diffusive wave field close to the free surface we expect the energy to be partitioned between body and Rayleigh waves (Weaver, 1985). Therefore, we can expect the value of R to lie between the ratio calculated for a pure body-wave field and the ratio calculated for the Rayleigh waves; we expect $6.5 < R < 10$.

Chilpancingo Array and Preliminary Data Processing

The choice of a convenient location was one of the critical points during the organization of the experiment, since we had to take into account different and sometimes contradictory factors. We wished to study the coda of regional and local earthquakes. Our measurements required signals with high signal-to-noise ratio and high quality of recordings. After considering these two points, we decided to deploy the array near the subduction zone of Mexico that is seismically a very active region (Singh *et al.,* 1983; Anderson *et al.,* 1989). An important requirement was to find a hard-rock site in order to minimize site effects and strong scattering due to the very superficial heterogeneities (Vernon *et al.,* 1998). Finally, we selected a site in the vicinity of the town of Chilpancingo (the capital of the state of Guerrero, Mexico). We installed four Guralp CMT40 sensors connected to Reftek 24-bit digitizers on a limestone hill. The absolute time was provided by the radio signals of GPS satellites. The array had the form of a square with a side length of ~50 m. It was operated between June and August 1997. During this period, we recorded 13 seismic events located at regional distances (from 50 to 460 km) and with magnitudes large enough to provide high signal-to-noise ratios. The locations of the events are shown in Figure 2 and their source parameters are listed in Table 1.

The precise configuration of the array is shown in Figure 3. Before applying equation (19), we made corrections to initial sensor orientations. The array was installed on a slope of 10 degrees, while the sensors were oriented horizontally. However, the system of equations (B2) requires the coordinate Z to be perpendicular to the free surface. Thus, the vertical components required rotation. Another problem occurred during the orientation of horizontal components of the sensors. One of the sensors (station 1) was installed at the site of a permanent accelerometric station and could be aligned with respect to the known orientation of the cabin where the permanent station is located. However, the other three sensors were aligned with a magnetic compass. Thus, the sensors could be oriented only very approximately. The errors in the sensor orientation can result in large errors in the calculation of the spatial derivatives. The following procedure was applied to correct the orientation errors. We took station 1 as the reference because of its well-defined orientation. We then selected an earthquake well recorded by all four sensors (event 2). The records were bandpassed between 0.1 and 0.5 Hz thus ensuring that the minimal wavelength was at least 10 times larger than the interstation distance. The stations were sufficiently close so that, for sensors with the same orientation, their records were expected to be

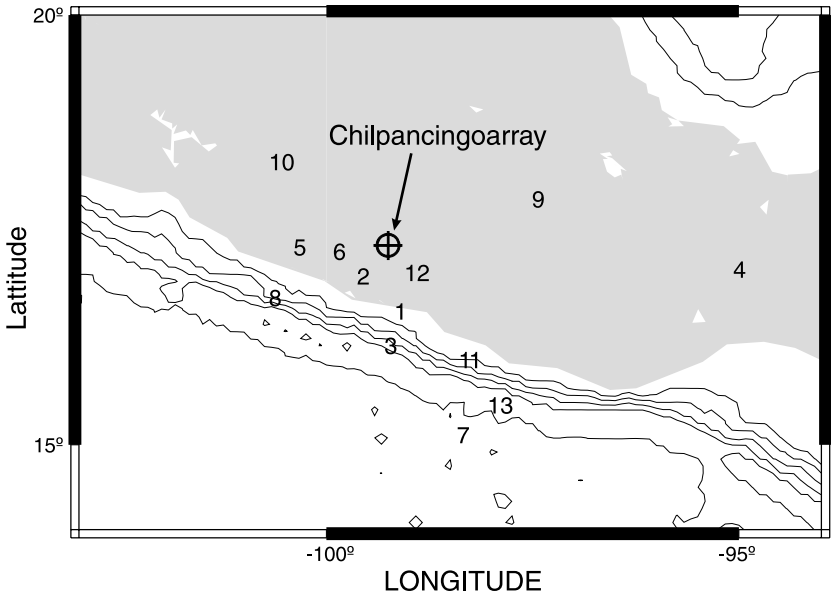

Figure 2. Map of Southern Mexico showing locations of the Chilpancingo array and the seismic events used in this study.

almost identical with the correlation coefficient of horizontal component records for any pair of stations equal to one. In the case of different orientations, these correlation coefficients would have been less than one. For each of stations 2, 3, and 4 we rotated horizontal-component records through angles from $-30°$ up to $30°$ with respect to initial orientation with a step of one degree. For each angle, we calculated the correlation coefficient of horizontal components with respect to the reference station. We oriented the sensors from the maximum value of the correlation coefficient (about 0.995 in our case).

After determination of exact orientations, we rotated the components to obtain a configuration shown in Figure 3, in which the coordinate Z is perpendicular to the surface and

Table 1
Parameters of Earthquakes Used in the Study

N?:	yy:mm:dd	lat	lon	H(km)	M	N
1	97:06:21	16.47	−99.18	5	4.5	3
2	97:06:28	16.88	−99.63	7	4.1	4
3	97:06:29	16.07	−99.30	23	4.4	4
4	97:06:29	16.96	−95.07	64	4.5	4
5	97:07:19	17.22	−100.4	56	4.9	3
6	97:07:21	17.17	−99.92	24	4.5	3
7	97:07:22	15.02	−98.42	5	5.1	3
8	97:07:24	16.63	−100.7	16	4.5	3
9	97:07:28	17.78	−97.51	126	4.0	4
10	97:07:29	18.21	−100.7	74	4.4	4
11	97:07:30	15.9	−98.4			4
12	97:08:01	16.92	−99.06	35	4.3	4
13	97:08:03	15.37	−98.05	27	4.7	4

Locations and magnitudes are given by the Mexican Seismological Service. N is a number of stations of the array that recorded the event.

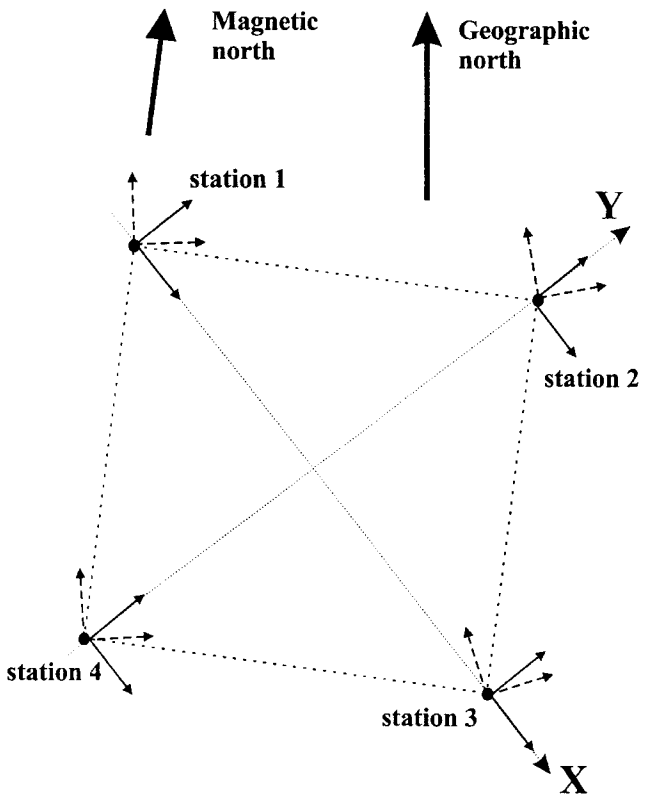

Figure 3. Configuration of the Chilpancingo array. Large arrows indicate directions of the magnetic and the geographic North. Small dashed and solid arrows show original and rotated orientation of horizontal components for each station.

coordinates X and Y are parallel to diagonals of the array. The last step was to integrate the velocity records to obtain the ground displacement. We estimated the spatial derivatives of the displacement at each point in time through these next equations:

$$\frac{\partial u_i}{\partial x} = \frac{u_i^3 - u_i^1}{d} \quad \frac{\partial u_i}{\partial y} = \frac{u_i^2 - u_i^4}{d} \quad i = x, y, z \tag{23}$$

where u_i^n is the displacement at station n of the array (see Fig. 4) and d is the distance between opposite stations of the array and is equal to 71 m. Some events were recorded only by three stations of the array (see Table 1). In this case, equations (23) were modified. For example, if the record at station 2 was absent, then spatial derivatives were calculated by the following expressions:

$$\begin{aligned} \frac{\partial u_i}{\partial x} &= \frac{u_i^3 - u_i^1}{d} \\ \frac{\partial u_i}{\partial y} &= \frac{u_i^1 + u_i^3 - 2u_i^4}{d} \quad i = x, y, z. \end{aligned} \tag{24}$$

The derivatives estimated from finite differences differ from exact values according to the relation

$$\frac{[\partial u_i/\partial x_j]_{\text{array}}}{[\partial u_i/\partial x_j]_{\text{exact}}} = \frac{\sin[\pi L/\lambda]}{\pi L/\lambda} \tag{25}$$

(Bodin *et al.,* 1997; Lomnitz, 1997), where L is the distance between receivers and λ is the wavelength. Since in our case $L/\lambda \leq 0.1$, the error in the measurement of the derivatives due to the use of finite differences is less then 2%. We performed a series of tests with synthetic seismograms that validated the procedure.

Experimental Results

After applying the corrections described in the previous section to the records of the 13 earthquakes listed in the Table 1, we measured the values of R using equations (19) and (23). For each record, we calculated the average value of R in a moving window of a 16-sec duration. We must recall here that the equilibration of the energies is a property of the average field. We may expect some fluctuations for a single realization. The window width has been selected to be of the order of the mean free time. The last one has been estimated using the mean free path of ~ 60 km proposed by Margerin *et al.* (1999) for the Mexican crust. The results of the processing of different events are shown in Figure 4. In some cases the ratio of energies stabilizes in the coda at a level very different from the ones in the noise and direct arrivals in a spectacular manner (as for events 2, 8, and 12). In other cases, we observe energy arrivals that produce fluctuations both for the coda decay and for R (e.g., around 300–350 sec for event 1). The important point in this study is not to interpret all the peculiarities of the records but to note the common behavior observed for all the records, beyond the specific fluctuations expected for multiply scattered waves in a random medium. We note that the ratio R remains relatively stable in the coda, but varies widely in the noise and at the onset of direct waves. The ratio does not vary more than about 25% of the mean value in the coda window, while at the same time, the energy decreases by a factor of 10,000. We present in Figure 5 the results of essentially the same analysis for events 8 and 12 but limited to the window of the direct arrivals of the body waves. Here, the mean value of the energy ratio R is calculated at 1-sec intervals. The evolution of R is now plotted on a logarithmic scale. R exhibits very rapid and large variations during the deterministic arrivals. This behavior is expected since the apparent P- and S-wave energies measured at the surface depend strongly on the incident angle (Fig. 1). We present this measure to show that the stabilization of R is actually a property of coda waves.

For all 13 earthquakes, we calculate an average value and a standard deviation of R in the whole coda window (shadowed areas in Fig. 4). The beginning of the coda window corresponds to the group velocity of 2.3 km/sec, which is clearly after the arrival of the direct S wave. The window ends when the energy is less then five times the noise level. We also measure R for first arrivals of S and P waves (shadowed areas in Fig. 5). The results of these measurements are presented in Figure 6 and indicate that R measured for direct waves varies by more than one order of magnitude from one event to another. This result is expected from the properties of reflection and conversion of body waves close to a free surface (Fig. 1). At the same time, R measured in the coda is very stable. For all events, it equals 7 ± 1.

Summarizing the observations, we find that energy ratio, R, has a very stable value along the whole coda window and it does not depend on the source location and magnitude. This stabilization of R in the coda is a strong indication that the diffusion regime has been reached. The equilibration between the different modes of vibration occurs rapidly in the coda. Only a few mean-free times are required to reach the partitioning. A qualitatively similar behavior has been found in the numerical simulations (Margerin *et al.,* 2000a) for the case of the Rayleigh-Gans scattering regime, that is, when the typical dimension of heterogeneity is of the order of the wavelength.

Conclusions

The measurements of the decay rate of the coda envelopes are insufficient to unambiguously distinguish different scattering regimes. Recently, the elastic radiative transfer equation has been derived (Papanicolaou *et al.,* 1996; Ryzhik *et al.,* 1996; Turner, 1998). This equation takes into account the wave polarization and the mode conversion between P and S waves, which occurs during each scattering event. These works show that, for long lapse time, the

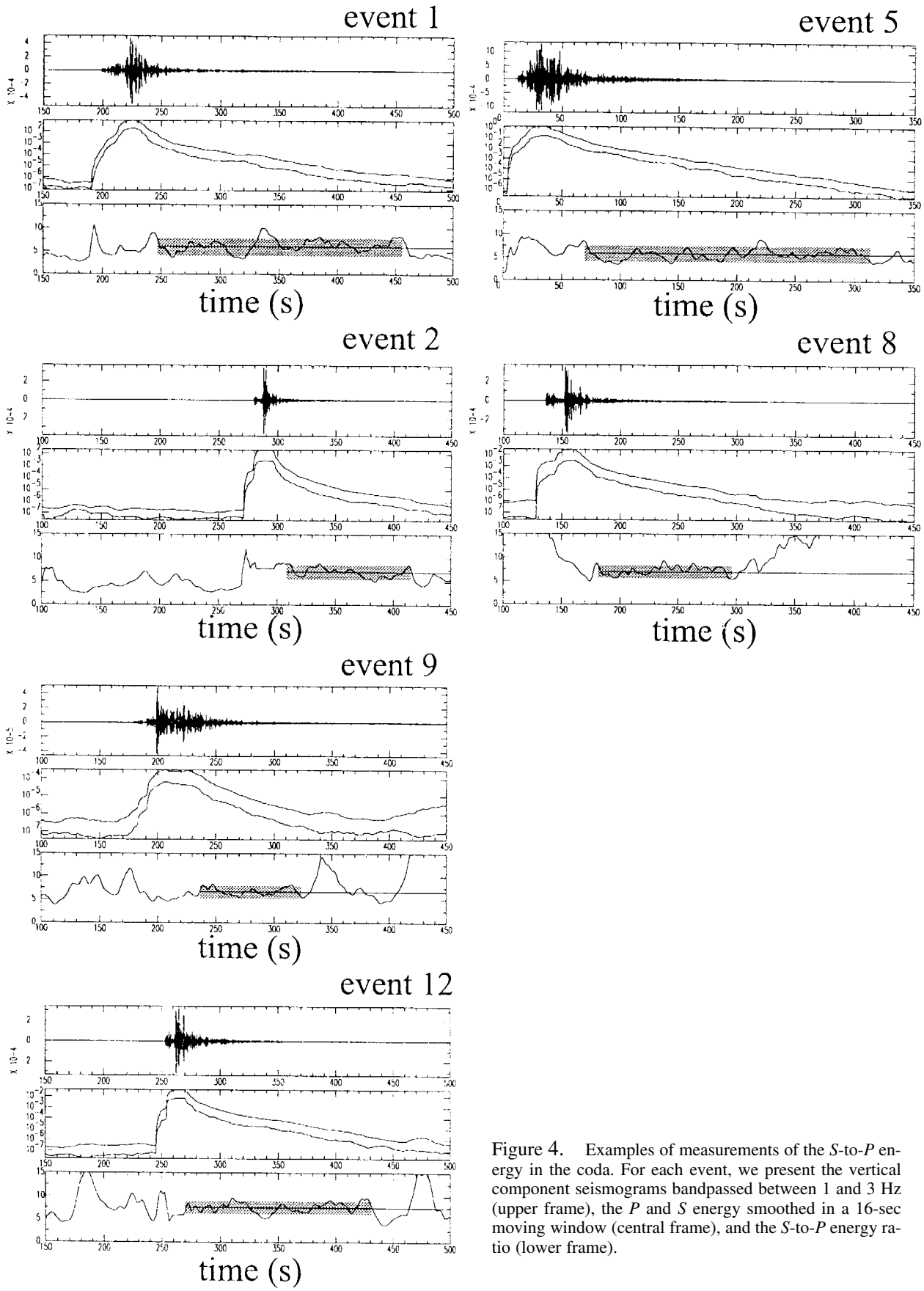

Figure 4. Examples of measurements of the *S*-to-*P* energy in the coda. For each event, we present the vertical component seismograms bandpassed between 1 and 3 Hz (upper frame), the *P* and *S* energy smoothed in a 16-sec moving window (central frame), and the *S*-to-*P* energy ratio (lower frame).

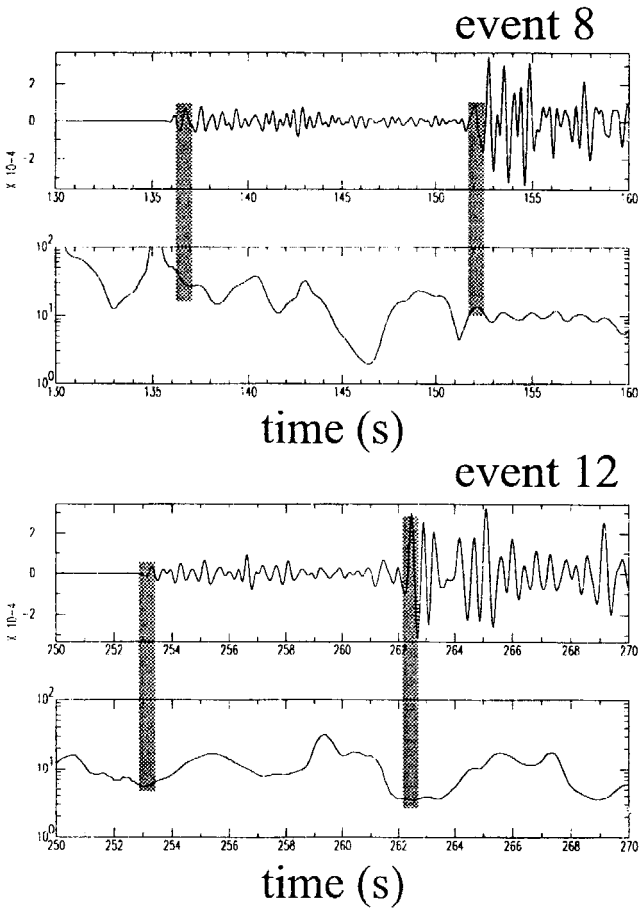

Figure 5. Examples of measurements of the *S*-to-*P* energy for direct waves for events 8 and 12. For each event, we present the vertical component seismograms bandpassed between 1 and 3 Hz (upper frame) and the *S*-to-*P* energy ratio (lower frame).

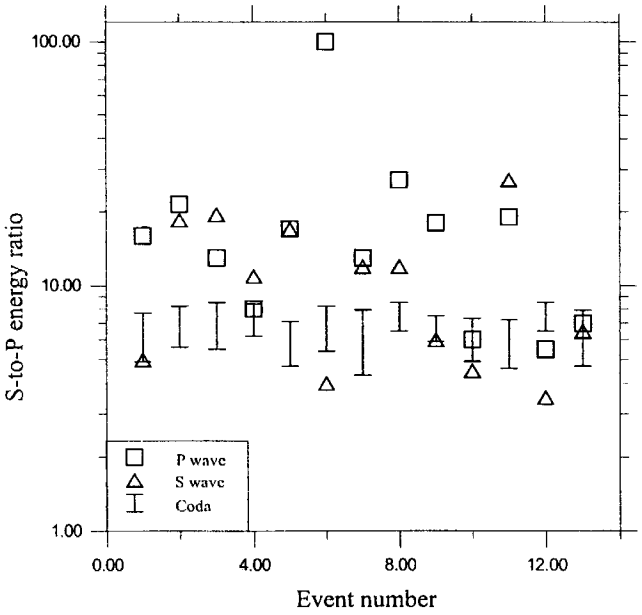

Figure 6. Measured *S*-to-*P* energy ratios for the 13 events. The squares and the triangles indicate the ratios measured during direct arrivals of *P* and *S* waves, respectively. Vertical bars show average values plus or minus the standard deviation of the *S*-to-*P* energy ratio measured in the coda window.

multiple-scattered intensities follow a simple diffusion equation, in spite of the existence of the two separate *P*- and *S*-propagation modes. In the diffusion regime in an infinite medium, the ratio of energy densities of *S* and *P* waves becomes constant. This energy partitioning was also obtained for short lapse times when solving the elastic radiative transfer equation using Monte Carlo method (Margerin *et al.,* 2000a). Close to the surface, the energy of the diffusive field is partitioned between body and surface waves (Weaver, 1985). It results in the energy partition between the curl and the divergence part of the wave field. In this article we propose to measure the curl-to-divergence energy ratio *R* to observe the energy partioning in the seismic coda. We applied our technique to the data of a small-aperture array operated during June–August 1997 in Guerrero (Mexico). During the three months of the experiment, we recorded 13 earthquakes with a good signal-to-noise ratio. For all events, the ratio *R* has been found to be very stable in the coda window, while the total energy level itself changes by several orders of magnitude. This ratio is also independent of the seismic source locations and magnitudes and it equals 7 ± 1. This value lies between the ratio expected for a purely Rayleigh wave field (6.5) and the one expected for a purely body-wave field (10). The partitioning regime is reached very fast (during few mean-free times). It indicates that the Rayleigh-Gans scattering regime is dominating; the typical dimension of heterogeneity is on the order of the wavelength.

Acknowledgments

We acknowledge financial support from Program "Interieur de la Terre" of INSU/CNRS (France), the European Union (contact CH*-CT92-0025), CONACYT, Mexico (projects 0974-PT, 27623-T, and J32308-T), and DGAPA, UNAM, Mexico (project IN109598). We thank B. Van Tiggelen, R. Maynard, and J. Turner for their help and suggestions, M. Fehler and two anonymous reviewers for the revision of the manuscript, and Enrique Guevara and German Espitia for their help in the installation and the operation of the Chilpancingo array.

References

Abubakirov, I. R., and A. A. Gusev (1990). Estimation of scattering properties of lithosphere of Kamchatka based on Monte-Carlo simulation of record envelope of a near earthquake, *Phys. Earth Planet. Interiors* **64,** 52–67.

Aki K. (1969). Analysis of the seismic coda of local earthquakes as scattered waves, *J. Geophys. Res.* **74,** 615–618.

Aki, K., and B. Chouet (1975). Origin of coda waves: source, attenuation, and scattering effects, *J. Geophys. Res.* **80,** 3322–3342.

Aki, K., and P. Richards, (1980). *Quantitative Seismology: Theory and Methods,* W. H. Freeman, New York 141.

Anderson, J. G., S. K. Singh, J. M. Espindola, and J. Yamamoto (1989).

Seismic strain release in the Mexican subduction thrust, *Phys. Earth Planet. Interiors* **58,** 307–322.

Bodin, P., J. Gomberg, S. K. Singh, and M. Santoyo (1997). Dynamic deformations of shallow sediments in the Valley of Mexico, Part I: three dimensional strains and rotations recorded on a seismic array, *Bull. Seism. Soc. Am.* **87,** 528–539.

Campillo, M., L. Margerin, and K. Aki (1998). Seismology, in *New Aspects of Electromagnetic and Acoustic Wave Diffusion,* POAN Research Group (Editor), Springer, New York, 87–99.

Campillo, M., L. Margerin, and N. M. Shapiro (1999). Seismic wave diffusion in the Earth lithosphere, in *Wave Diffusion in Complex Media,* ASI Series, J. P. Fouque (Editor), Kluwer, Hingham, Massachusetts 383–403.

Dainty, A. M., and M. N. Toksoz (1990). Array analysis of seismic scattering, *Bull. Seism. Soc. Am.* **80,** 2248–2260.

Gusev, A. A. (1995). Vertical profile of turbidity and coda Q, *Geophys. J. Int.* **123,** 665–672.

Hoshiba, M. (1991). Simulation of multiple scattered coda wave excitation based on the energy conservation law, *Phys. Earth Planet. Interiors* **67,** 126–136.

Hoshiba, M. (1997). Seismic coda wave envelope in depth dependent *S*-wave velocity structure, *Phys. Earth Planet. Interiors* **104,** 15–22.

Lomnitz, C. (1997). Frequency response of a strainmeter, *Bull. Seism. Soc. Am.* **87,** 1078–1080.

Margerin, L., M. Campillo, and B. A. Van-Tiggelen (1998). Radiative transfer and diffusion of waves in a layered medium: a new insight into coda Q, *Geophys. J. Int.* **134,** 596–612.

Margerin, L., M. Campillo, N. M. Shapiro, and B. A. Van-Tiggelen (1999). The time of residence of diffuse waves in the crust and the physical interpretation of coda Q, *Geophys. J. Int.* **138,** 343–352.

Margerin, L., M. Campillo, and B. A. Van-Tiggelen (2000a). Monte Carlo simulation of multiple scattering of elastic waves, *J. Geophys. Res.* **105,** 7873–7892.

Margerin, L., B. A. Van-Tiggelen, and M. Campillo (2000b). Effect of absorption on the energy partitioning of coda waves, *Bull. Seism. Soc. Am.* (submitted for publication).

Papanicolaou, G. C., L. V. Ryzhik, and J. B. Keller (1996). Stability of the *P* to *S* ratio in the diffusive regime, *Bull. Seism. Soc. Am.* **86,** 1107–1115.

Ryzhik, L. V., G. C. Papanicolaou, and J. B. Keller (1996). Stability of the *P* to *S* ratio in the diffusive regime, *Wave Motion* **24,** 327–370.

Sato, H., and M. C. Fehler (1998). Seismic wave propagation and scattering in the heterogeneous Earth, in *ATP Series in Modern Acoustics and Signal Processing,* Springer, New York.

Singh, S. K., M. Rodriguez, and L. Esteva (1983). Statistics of small earthquakes and frequency of occurrence of large earthquakes along the Mexican subduction zone, *Bull. Seism. Soc. Am.* **73,** 1779–1796.

Spudich, P. L., L. K. Steck, M. Helweg, J. B. Fletcher, and L. M. Baker (1995). Transient stress at Parkfield, California, produced by the *M* 7.4 Landers earthquake of 28 June 1992: observations from the UPSAR dense seismograph array, *J. Geophys. Res.* **100,** 675–690.

Turner, J. A. (1998). Scattering and diffusion of seismic waves, *Bull. Seism. Soc. Am.* **88,** 276–283.

Vernon, F. L., G. L. Pavlis, T. J. Owens, D. E. McNamara, and P. N. Anderson (1998). Near-surface scattering effects observed with a high-frequency phased array at Pinyon Flats, California, *Bull. Seism. Soc. Am.* **88,** 1548–1560.

Weaver, R. L. (1982). On diffuse waves in solid media, *J. Acoust. Soc. Am.* **71,** 1608–1609.

Weaver, R. L. (1985). On diffuse waves at a free surface, *J. Acoust. Soc. Am.* **78,** 136–131.

Weaver, R. L. (1990). Diffusivity of ultrasound in polycrystals, *J. Mech. Phys. Solids* **38,** 55–86.

Wu, R. S. (1985). Multiple scattering and energy transfer of seismic waves: separation of scattering effect from intristic attenuation, I, theoretical modelling, *Geophys. J. R. Astr. Soc.* **82,** 57–80.

Appendix A: Energy of a Random and Isotropic Seismic Wave Field

In an isotropic medium, the energy of deformation, W, equation (6) can be rewritten:

$$W = \frac{K}{2}\chi_{ll}^2 + \mu\left(\chi_{ij} - \frac{1}{3}\delta_{ij}\chi_{ll}\right)^2 = \frac{\lambda}{2}\chi_{ll}^2 + \mu\chi_{ij}^2 \quad \text{(A1)}$$

where

$$K = \lambda + \frac{2}{3}\mu. \quad \text{(A2)}$$

λ and μ are the Lame constants, χ and σ are the strain and stress tensors, respectively. χ_{ij} can be written as

$$\chi_{ij} = \frac{1}{2}(u_{ij} + u_{ji}) \quad \text{(A3)}$$

where u_{ij} is the derivative of the ith component of the displacement with respect to the jth coordinate. After this substitution and a recombination of terms we obtain:

$$W = \left(\frac{\lambda}{2} + \mu\right)(\mathrm{div}\,\vec{u})^2 + \frac{\mu}{2}(\mathrm{curl}\,\vec{u})^2 + \mu I \quad \text{(A4)}$$

where

$$I = 2\left(\frac{\partial u_x}{\partial y}\frac{\partial u_y}{\partial x} + \frac{\partial u_x}{\partial z}\frac{\partial u_z}{\partial x} + \frac{\partial y_y}{\partial z}\frac{\partial u_z}{\partial y}\right) - 2\left(\frac{\partial u_x}{\partial x}\frac{\partial u_y}{\partial y} + \frac{\partial u_x}{\partial x}\frac{\partial u_z}{\partial z} + \frac{\partial u_y}{\partial y}\frac{\partial u_z}{\partial z}\right). \quad \text{(A5)}$$

Let us now consider a random and isotropic wave field as a sum of *a priori* noncorrelated plane P and S waves coming from different directions:

$$\vec{u} = \sum_{i_P}\vec{U}_{i_P}^P + \sum_{i_s}\vec{U}_{i_s}^S. \quad \text{(A6)}$$

The energy density of an individual P wave is

$$W_{i_P} = \left(\frac{\lambda}{2} + \mu\right)(\mathrm{div}\vec{U}_{i_P}^P)^2 \quad \text{(A7)}$$

and of a S wave is

$$W_{i_s} = \frac{\mu}{2}(\mathrm{curl}\vec{U}_{i_s}^S)^2. \quad \text{(A8)}$$

Let us now calculate the average energy in sufficiently large time window $\bar{W}$. In a random wave field, the displacement components are not correlated. As a consequence, the term I vanishes:

$$\bar{I} = 0 \tag{A9}$$

and equation (A4) becomes:

$$\bar{W} = \overline{\left(\frac{\lambda}{2} + \mu\right)(\mathrm{div}\,\vec{u})^2} + \overline{\frac{\mu}{2}(\mathrm{curl}\,\vec{u})^2}. \tag{A10}$$

Now we substitute equations (4), (5), (A6), (A7), and (A8) in equation (A10). Since the individual waves are not correlated, the average of terms like $div\vec{U}_i^P\ div\vec{U}_j^P$ and $(curl\vec{U}_i^P,\ curl\vec{U}_j^P)$ becomes zero and we can write

$$\overline{\left(\frac{\lambda}{2} + \mu\right)(\mathrm{div}\,\vec{u})^2} = \sum_{i_\mathrm{P}} \overline{W_{i_\mathrm{P}}} \tag{A11}$$

and

$$\overline{\frac{\mu}{2}(\mathrm{curl}\,\vec{u})^2} = \sum_{i_\mathrm{s}} \overline{W_{i_\mathrm{s}}}. \tag{A12}$$

Therefore the average energy can be written as a sum of *P*- and *S*-wave energies:

$$\bar{W} = \overline{W_P} + \overline{W_S} \tag{A13}$$

where

$$\overline{W_P} = \sum_{i_\mathrm{P}} \overline{W_{i_\mathrm{P}}} = \overline{\left(\frac{\lambda}{2} + \mu\right)(\mathrm{div}\,\vec{u})^2} \tag{A14}$$

$$\overline{W_S} = \sum_{i_\mathrm{s}} \overline{W_{i_\mathrm{p}\to i_\mathrm{s}}} = \overline{\frac{\mu}{2}(\mathrm{curl}\,\vec{u})^2}. \tag{A15}$$

Appendix B: Spatial Derivatives with Respect to Z

The boundary condition of zero traction at a free surface is:

$$\sigma_{xz} = 0 \quad \sigma_{yz} = 0 \quad \sigma_{zz} = 0. \tag{B1}$$

In an isotropic medium, the equation (B1) can be written as

$$\begin{cases} \dfrac{\partial u_\mathrm{y}}{\partial z} + \dfrac{\partial u_\mathrm{z}}{\partial y} = 0 \\ \dfrac{\partial u_\mathrm{x}}{\partial z} + \dfrac{\partial u_\mathrm{z}}{\partial x} = 0 \\ \lambda\left(\dfrac{\partial u_\mathrm{x}}{\partial x} + \dfrac{\partial u_\mathrm{y}}{\partial y}\right) + (\lambda + 2\mu)\dfrac{\partial u_\mathrm{z}}{\partial z} = 0, \end{cases} \tag{B2}$$

which gives derivatives with respect to z:

$$\begin{cases} \dfrac{\partial u_\mathrm{y}}{\partial z} = -\dfrac{\partial u_\mathrm{z}}{\partial y} \\ \dfrac{\partial u_\mathrm{x}}{\partial z} = -\dfrac{\partial u_\mathrm{z}}{\partial x} \\ \dfrac{\partial u_\mathrm{z}}{\partial z} = -\dfrac{\lambda}{\lambda + 2\mu}\left(\dfrac{\partial u_\mathrm{x}}{\partial x} + \dfrac{\partial u_\mathrm{y}}{\partial y}\right). \end{cases} \tag{B3}$$

Using equations (10), (11), and (B3) we can now estimate the entire set of spatial derivatives of the displacement. The equations (10) and (11) can be rewritten as

$$\frac{W_S}{W_P} = \frac{1}{4}\left(\frac{\alpha}{\beta}\right)^2 \frac{\overline{4\left(\dfrac{\partial u_\mathrm{x}}{\partial x}\right)^2 + 4\left(\dfrac{\partial u_\mathrm{x}}{\partial y}\right)^2 + \left(\dfrac{\partial y_\mathrm{x}}{\partial y} - \dfrac{\partial u_\mathrm{y}}{\partial x}\right)^2}}{\overline{\left(\dfrac{\partial u_\mathrm{x}}{\partial x} + \dfrac{\partial u_\mathrm{y}}{\partial y}\right)^2}}. \tag{B4}$$

Instituto de Geofísica
Universidad National Autónoma de México
México D.F., Mexico
(N. M. S., S. K. S., V. K., J. P.)

Laboratoire de Géophysique Interne et Tectonophysique
UMR CNRS 5559
Université Joseph Fourier
Grenoble, France
(M. C., L. M.)

Manuscript received 12 February 1999.